# Tropospheric vertical column densities of $NO_2$ over managed dryland ecosystems (Xinjiang, P. R. China): MAX-DOAS measurements vs. 3-D dispersion model simulations based on laboratory derived NO emission from soil samples

Buhalqem Mamtimin[1]*, Thomas Behrendt[1], Moawad M. Badawy[1,2], Thomas Wagner[3], Yue Qi[1,4], Zhaopeng Wu[1,5] and Franz X. Meixner[1]

[1]*Biogeochemistry Department, Max Planck Institute for Chemistry, Mainz, Germany.*
[2]*Department of Geography, Faculty of Arts, Ain-Shams University, Egypt.*
[3]*Air Chemistry Department, Max Planck Institute for Chemistry, Mainz, Germany.*
[4] *International Cooperation Department, National Center for Climate Change Strategy and International Cooperation, Beijing, P. R. China.*
[5]*Institute of Geography Science, Xinjiang Normal University, China,*

*Corresponding author: buhalqem.mamtimin@mpic.de

**Abstract**

We report on MAX-DOAS observations of $NO_2$ over an oasis-ecotone-desert ecosystem in NW-China. There, local ambient $NO_2$ concentrations originate from enhanced biogenic NO emission of intensively managed soils. Our target oasis "Milan" is located at the southern edge of the Taklimakan desert, very remote and well isolated from other potential anthropogenic and biogenic $NO_x$ sources. Four observation sites for MAX-DOAS measurements were selected, at the oasis center, downwind and upwind of the oasis, and in the desert. Biogenic NO emissions in terms of (i) soil moisture and (ii) soil temperature of Milan oasis' (iii) different land-cover type sub-units (cotton, Jujube trees, cotton/Jujube mixture, desert) were quantified by laboratory incubation of corresponding soil samples. Net potential NO fluxes were up-scaled to oasis scale by areal distribution and classification of land-cover types derived from satellite images using GIS techniques. A Lagrangian dispersion model (LASAT, Lagrangian Simulation of Aerosol-Transport) was used to calculate the dispersion of soil emitted NO into the atmospheric boundary layer over Milan oasis. Three dimensional NO concentrations (30 m horizontal resolution) have been converted to 3-D (three dimensional) $NO_2$ concentrations, assuming photostationary state conditions. $NO_2$ column densities were simulated by suitable vertical integration of modeled 3-D $NO_2$ concentrations at those downwind and upwind locations, where the MAX-DOAS measurements were performed. Downwind-upwind differences (a direct measure of Milan oasis' contribution to the areal increase of ambient $NO_2$ concentration) of measured and simulated slant (as well as vertical) $NO_2$ column densities show excellent agreement. This agreement is considered as the first successful attempt to prove the validity of the chosen approach to up-scale laboratory derived biogenic NO fluxes to ecosystem field conditions, i.e. from the spatial scale of a soil sample ($cm^2$) to the size of an entire agricultural ecosystem ($km^2$).

## 1 Introduction

Emissions of nitric oxide (NO) are important in regulating chemical processes of the atmosphere (Crutzen, 1987). Once emitted into the atmosphere, NO reacts rapidly with ozone ($O_3$) to nitrogen dioxide ($NO_2$) which, under daylight conditions, is photolyzed back to NO ($\lambda \leq$ 420 nm). For that reason, NO and $NO_2$ are usually considered as $NO_x$ ($NO_x = NO + NO_2$). Ambient $NO_x$ is a key catalyst in atmospheric chemistry: during the atmospheric oxidation of hydrocarbons its ambient concentration determines whether ozone ($O_3$) is photochemically generated or destroyed in the troposphere (Chameides et al., 1992). While the combustion of fossil fuels (power plants, vehicles) is still the most important global $NO_x$ source (approx. 25 Tg $a^{-1}$ in terms of mass of N), biogenic NO emissions from soils have been estimated to range between 6.6 and 9.6 Tg $a^{-1}$ (Denman et al., 2007). The considerable uncertainty about the range of soil biogenic NO emissions stems from widely differing estimates of the NO emission. Moreover, the uncertainties in the NO emission data from semi-arid, arid, and hyper-arid regions are very large (mainly due to a very small number of measurements being available). These ecosystems, however, are considered to contribute more than half to the global soil NO source (Davidson and Kingerlee, 1997), and make approx. 40% of planet Earth's total land surface (Harrison and Pearce, 2000).

Production (and consumption) of NO in the soil depends mainly on soil microbial activity and is mainly controlled by soil temperature, soil moisture, and soil nutrient concentration (Conrad, 1996; Meixner and Yang 2006; Ludwig et al., 2001). Any natural or anthropogenic action that result in the inputs of nutrients (e.g. by fertilizer application) and/or modification of soil nutrient turnover rates has a substantial effect on soil biogenic NO emission. The rapid (economically driven) intensification of arid agriculture (oasis agriculture), particularly by enlargement of the arable area and by enhancement of necessary irrigation leads inevitably to the increase of soil biogenic NO emissions. Since those microbial processes which underlay NO production and NO consumption in soils are confined to the uppermost soil layers (<0.0 5 m depth, Rudolph et al., 1996), the most direct method for their characterization and quantification is usually realized by laboratory incubation of soil samples; corresponding measurements result in the determination of so-called net potential NO fluxes, which are explicit functions of soil moisture, soil temperature, and ambient NO concentration (Behrendt et al., 2014).

Tropospheric $NO_2$ column densities can be retrieved from satellite observations using differential optical absorption spectroscopy (DOAS) (e.g. Leue et al., 2001; Richter and

Burrows, 2002, Beirle et al., 2004). Identification and quantification of the sources of tropospheric $NO_2$ column densities are important for monitoring air quality, for understanding radiative forcing and its impact on local climate. Ground-based Multi Axis Differential Optical Absorption Spectroscopy (MAX-DOAS) is a novel measurement technique (Hönninger et al., 2004) that represents a significant advantage over the well-established zenith scattered sunlight DOAS instruments, which are mainly sensitive to stratospheric absorbers. From $NO_2$ slant column densities, retrieved from measurements at different elevation angles, information about tropospheric $NO_2$ profiles and/or tropospheric vertical column densities can be obtained (e.g. Sinreich et al., 2005; Wittrock et al., 2004; Wagner et al., 2011).

In this paper we concentrate (a) on ground-based MAX-DOAS measurements of slant and vertical $NO_2$ column densities over an intensively used oasis of the Taklimakan desert (NW-China), (b) on biogenic NO emissions derived from laboratory incubation measurements on oasis soil samples, (c) on up-scaling of the laboratory results to the oasis level, (d) calculation of atmospheric boundary layer $NO_2$ concentrations by suitable $NO \rightarrow NO_2$ conversion and 3 dimensional dispersion modelling, and (e) on simulating slant and vertical $NO_2$ column densities from the calculated 3-D-$NO_2$ distributions by integration along the MAX-DOAS light path. The final aim is comparison and discussion of the results obtained under (a) and (e).

## 2 Materials and methods

### 2.1 Research area

After two 'searching field campaigns' (2008 and 2009) in the Xinjiang Uighur Autonomous Region of NW-China, the oasis "Milan" has been identified as the target oasis for the presented research. The contemporary oasis Milan, identical to the ancient silk-road post "Miran", belongs to the county "Ruoqiang" of the Xinjiang province and is located in the southern Taklimakan Desert on the foot of the Altun Shan Mountains (39.25 °N, 88.92 °E, 998 m a.s.l.). In the early 1950s, the delta-shaped oasis (see Fig. 1) has been established as an agricultural co-operative "state farm" (*Xinjiang Production and Construction Crop*) and covers nowadays about 100 $km^2$. Milan oasis can be geomorphologically classified as a "mountain-oasis-ecotone-desert system (MOED system)" consisting of Gobi (gravel) desert, a salty transition zone surrounding the oasis, and dryland farming with irrigation. The latter consists only of two crops, cotton and jujube trees (*Ziziphus Jujuba* L., "*red date*"), which are planted, irrigated, and fertilized following standardized protocols and growing on rectangular

fields (approx. 10 ha) of pure cultures or mixtures of it. The general energy supply of Milan oasis is entirely provided by nearby hydropower plants, and battery powered trikes dominate the local public and private transport. Consequently, anthropogenic $NO_x$ emissions of Milan oasis are considered as very low, if not negligible. Beyond that, Milan oasis is isolated by the desert from neighbouring oases by 80 to 400 km. Therefore, the dominant $NO_x$ source of Milan oasis are biogenic NO emissions from its intensively managed crop fields; the oasis can be undoubtedly considered as a large "hotspot in the middle of nothing". Given this very specific situation, it is certainly justified to assume that (a) $NO_2$ concentrations in the atmospheric boundary layer over Milan oasis are only caused by the oasis itself, and (b) free tropospheric $NO_2$ concentrations, which are usually due to large-scale tropospheric $NO_2$ advection, are negligible.

According to Koeppen classification (Koeppen, 1931; Kottek et al., 2006), Milan oasis owns a cold desert climate (BWk), which is dominated by long hot summers (30 years' mean: 29°C) and cold winters (30 years' mean: – 6°C). Mean annual precipitation amounts 28.5 mm, mean annual evaporating capacity is 2920 mm, mean wind direction is NE to E, and mean wind speed is 2.7 m $s^{-1}$.

## *2.2 In-situ* measurements

A field campaign has been performed at Milan oasis, from 24 May to 26 June, 2011. A total of 32 individual MAX-DOAS measurements (approx. 20 min) have been performed by two Mini-MAX-DOAS instruments (partially simultaneously) on 21 days during the 2011 campaign at the NE natural forest site (1), desert site (2), jujube site (3) and hotel station in Milan oasis center (4). Accompanying data of wind direction, wind speed, air temperature, barometric pressure, global and net radiation have been observed at sites (1) – (5) at 1.8 m above ground (at NE natural forest: 11 m; at hotel station: 23 m). Soil temperature (at 0.05 m depth), as well as rainfall (amount and intensity) were recorded at all sites in 2011.

### 2.2.1 Ground-based measurements of vertical column densities of $NO_2$

Multi-Axis-Differential Optical Absorption Spectroscopy (MAX-DOAS) observes scattered sun light under various (mostly slant) elevation angles. From combinations of the retrieved $NO_2$ slant column densities (SCDs) obtained at different elevation angles, information on the vertical $NO_2$ profile and/or on the corresponding vertical column density (VCD) can be obtained (e.g. Hönninger et al., 2002; Sinreich et al., 2005; Wittrock et al., 2004; Wagner et al., 2011). Spectral calibration of the MAX-DOAS instruments was performed by fitting a

measured spectrum to a convoluted solar spectrum based on a high resolution solar spectrum (Kurucz et al., 1984). Several trace gas absorption cross sections of $NO_2$ at 294 K (Vandaele et al., 1996), $H_2O$ at 290 K (Rothman et al., 2005), Glyoxal at 296 K (Volkamer et al., 2005), $O_3$ at 243 K (Bogumil et al., 2003) and $O_4$ at 286K (Hermans et al., 1999) were convolved to match the resolution of the instrument and then used in the spectral analysis using a wavelength range of 420-450 nm (also a Ring spectrum was included in the fitting process). The output of the spectral analysis is the $NO_2$ SCD, which represents the $NO_2$ concentration integrated along the corresponding light paths through the atmosphere.

Since a spectrum measured in zenith direction (a so called Fraunhofer reference spectrum) is included in the fit process to remove the strong Fraunhofer lines, the retrieved $NO_2$ SCD actually represents the difference between the SCDs of the measurement and the Fraunhofer reference spectrum; it is usually referred to as differential SCD or $DSCD_{meas}$. The tropospheric DSCD for the elevation angle α can be derived from MAX-DOAS observation by subtracting the $NO_2$ DSCD for the closest zenith observation ($\alpha_0 = 90°$):

$$DSCD_{trop}(\alpha) = DSCD_{meas}(\alpha) - DSCD_{meas}(\alpha_0) \quad (1)$$

DSCDs are converted into VCDs (the vertically integrated concentration) using so called air mass factors (AMF, Solomon et al., 1987), which is defined by:

$$AMF = SCD / VCD \quad (2)$$

In many cases AMF are determined from radiative transfer simulations (Solomon et al., 1987). However, if trace gas column densities are retrieved from MAX-DOAS observations at high elevation angles (> 10°), the AMF can be determined by the so called geometric approximation (Hönninger et al., 2002; Brinksma et al., 2008; Wagner et al., 2010):

$$AMF_{trop} \approx \frac{1}{\sin(\alpha)} \quad (3)$$

In this study, the tropospheric vertical column density ($VCD_{trop}$) is obtained from $DSCD_{trop}(\alpha)$ as discussed by Wagner et al. (2010):

$$VCD_{trop} = \frac{DSCD_{trop}(\alpha)}{AMF_{trop}(\alpha - AMF_{trop}(\alpha_0))} \quad (4)$$

During the field experiments, the MAX-DOAS instruments have been mounted on solid tables (aluminium structure) at approx. 11 m a.gr. (NW natural forest, hotel station) and 3.5 m a.gr. (remainder of sites) with the telescope facing northwards. Observations were always made on elevation angles of 0°, 2°, 4°, 6°, 8°, 10°, 15°, 20°, 45° and 90°. $VCD_{trop}$s were determined from measurements at 15°. The potential importance of scattering on the interpretation of the MAX-DOAS measurements depends on two main aspects: first on the height of the trace gas layer and second on the amount of aerosols. In our case the trace gas layer is shallow and the aerosol amount is low (see 2.2.8). Thus scattering effects can be neglected. However, for comparison of the $DSCD_{trop}$ data obtained by MAX-DOAS with the simulated SCDs obtained from 3 D distributions of $NO_2$ concentration (calculated with LASAT (Lagrangian Simulation of Aerosol-Transport)) on the basis of laboratory derived net potential $NO_2$ fluxes) the lower elevation angles (2°, 4°) for $DSCD_{trop}(\alpha)$ have been used, which have a much higher sensitivity to the observed $NO_2$.

For classifying all MAX-DOAS measurements whether they were made up-wind, down-wind, or in the center of Milan oasis, their observation position was related to the mean wind direction during each measurement period. Wind measurements were part of accompanying *in-situ* measurements (see below).

### 2.2.2 Accompanying measurements

Wind direction, wind speed, air temperature, relative humidity, barometric pressure, and rainfall intensity have been measured by combined weather sensors (weather transmitter WXT510, Vaisala, Finland). All five weather sensors have been operated side-by-side for one week before they have been mounted at the individual measurement sites (1) – (5). Based on these results, all meteorological data, which have been measured between 3 – 24 July, 2011 have been corrected using one of the sensors as reference. All combined weather sensors' data, as well as those of net radiation (4 component net radiation sensor, model NR01, Hukseflux, The Netherlands) and soil temperature (thermistor probe, model 109, Campbell Scientific, U.S.A.) have been recorded every minute. Ambient $O_3$ concentrations and $NO_2$ photolysis rates have also been measured in-situ; both quantities are necessary to calculate the $NO \rightarrow NO_2$ conversion factor (see Sect. 2.2.8). Ozone concentrations have been measured by UV-absorption spectroscopy (model 49i, ThermoFisher Scientific, U.S.A.) and $NO_2$ photolysis rate by a filter radiometer (model 2-Pi-$JNO_2$, metcon, Germany) in 1 minute intervals.

### 2.2.3 Soil samples

Microbial processes responsible for biogenic NO emission are confined to the uppermost soil layers (Galbally and Johansson, 1989; Rudolph et al., 1996; Rudolph and Conrad, 1996). Consequently, composite soil samples (1 kg of top soil, 0–5 cm depth) have been collected at the individual sites of Milan oasis (natural forest, cotton, jujube, cotton & jujube mixture, desert). All samples (air dried) were sent from Xinjiang to Germany by air cargo and stored refrigerated (+ 4°C) until laboratory analysis of the net potential NO flux (see below). Sub-samples have been analyzed for dry bulk soil density (ISO 11272), pH (ISO 10390), electrical conductivity (salinity, ISO 11265), contents of nitrate and ammonium (ISO 14256), total carbon and total nitrogen (ISO 10649 and ISO 13878), texture (ISO 11277), as well of soil water potential (pF values 1.8, 2.5, 4.2, Hartge and Horn, 2009).

Electrical conductivity varied between 1.6 to 9.5 dS $m^{-1}$ within the managed soils, and was 59.8 and 3.0 dS $m^{-1}$ in the natural forest and desert soils, respectively. Commercially available soil moisture probes (e.g. TDR (Time-Domain-Reflectometry) and FDR (Frequence-Domain-Reflectometry)) show extreme interferences for soils of >2 dS $m^{-1}$ (c.f. Kargas et al., 2013) and their calibration for such soils is extremely challenging, if possible at all. Indeed, FDR-signals monitored in Milan oasis' soils were extremely noisy and spurious. Nevertheless, up-scaling of the laboratory derived net potential NO fluxes needs data of the uppermost layer of each soil of Milan oasis land-types (see Sect. 2.2.6). For that, as most reasonable approximation, it was decided to use that individual (constant) gravimetric soil moisture content, which corresponds to the so-called "wilting point". The latter was determined by laboratory water tension measurements (pF 4.2) on undisturbed soil cores from each land-cover type. The wilting point is defined as that soil moisture in the root zone, which would cause irreversible wilting of plants. Wilting point conditions in the uppermost soil layers (2 cm) of soils in the Taklimakan Desert are easily reached, since evaporation is extremely high (evaporating capacity 2920 mm $a^{-1}$). Even after flooding irrigation of Milan oasis' crop fields, these conditions have repeatedly been observed within at least 3 days by visual inspections.

### 2.2.4 Laboratory determination of net potential NO fluxes

The methodology for the laboratory measurement of the NO flux from soil has been developed at the end of the nineties (Yang and Meixner, 1997) and has been continuously used during the last two decades (Otter et al., 1999; Kirkman et al., 2001; van Dijk and Meixner, 2001; Feig et al., 2008a; Feig et al., 2008b; Yu et al., 2008; Ashuri, 2009; Feig, 2009; Gelfand et al., 2009; Yu et al., 2010a, 2010b; Bargsten et al., 2010). The methodology has been

significantly improved in the frame of this study and is described in detail by Behrendt et al. (2014).

Generally, the release of gaseous NO from soil is the result of microbial NO production and simultaneous NO consumption. The latter is, as shown by Behrendt et al. (2014), particularly for arid and hyper-arid soils, negligible. Applying the laboratory dynamic chamber method, the release of NO is determined by incubating aliquots of the soil samples in a dynamic chamber system under varying, but prescribed conditions of soil moisture, soil temperature, and chamber's headspace NO concentrations. From the difference of measured NO concentrations at the outlets of each soil containing chamber and an empty reference chamber, actual net potential NO fluxes (in terms of mass of nitric oxide per area and time) is calculated as function of soil moisture and soil temperature. For that, a known mass (approx. 60 g dry weight) of sieved (2 mm) and wetted (to water holding capacity) soil is placed in one of six Plexiglas chambers (volume $9.7 \times 10^{-4}$ $m^3$) in a thermo-controlled cabinet (0 – 40°C). After passing through a purification system (PAG 003, Ecophysics, Switzerland), dry pressurized, zero (i.e., "NO free") air is supplied to each chamber, controlled by a mass flow controller ($4.167 \times 10^{-5}$ $m^3$ $s^{-1}$). The outlet of each chamber is connected via a switching valve system to the gas-phase chemiluminescence NO analyzer (model 42i-TL, Thermo Fisher Scientific Inc., U.S.A.) and to the non dispersive infrared analyzer $CO_2$/$H_2O$-analyzer (model LI-COR 840A, LI-COR Biosciences Inc., U.S.A.). During a period of 24 – 48 h, the soil samples are slowly drying out, hence providing the desired variation over the entire range of soil moisture (i.e. from water holding capacity to wilting point conditions and completely dry soil). During the drying out period, the temperature of thermo-controlled cabinet is repeatedly changed from 20 to 30°C, hence providing the desired soil temperature variation (Behrendt et al. 2014). Occasionally, nitric oxide standard gas (200 ppm) is diluted into the air purification system via a mass flow controller; this allows the control of the chamber headspace NO concentration when determining NO consumption rate of the soil sample. The actual soil moisture content of each soil sample is determined by considering the $H_2O$ mass balance of each chamber, where the temporal change of the chamber's headspace $H_2O$ concentration is explicitly related to the evaporation rate of the soil sample. Tracking the chamber's headspace $H_2O$ concentration throughout the drying-out period and relating it to the gravimetrically determined total soil mass at the start and end of the measurement period delivers the actual gravimetric soil moisture content of the soil sample (Behrendt et al., 2014).

As shown during the last two decades (Yang and Meixner, 1997; Otter et al., 1999; Kirkman et al., 2001; van Djik and Meixner, 2001; van Dijk et al., 2002; Meixner and Yang, 2006; Yu

et al., 2008, 2010; Feig et al., 2008; Ashuri, 2009; Feig, 2009; Gelfand et al., 2009 and Bargsten et al., 2010), the dependence of NO release from gravimetric soil moisture and soil temperature can be characterized by two explicit dimensionless functions, the so-called optimum soil moisture curve $g(\theta_g)$ and the exponential soil temperature curve $h(T_{soil})$

$$g(\theta_g) = \left(\frac{\theta_g}{\theta_{g,0}}\right)^a \exp\left[-a\left(\frac{\theta_g}{\theta_{g,0}} - 1\right)\right] \quad (5)$$

$$h(T_{soil}) = \exp\left[\frac{\ln Q_{10,NO}}{10}\left(T_{soil} - T_{soil,0}\right)\right] \quad (6)$$

where $\theta_g$ is the dimensionless gravimetric soil moisture content, $\theta_{g,0}$ the so-called optimum gravimetric soil moisture content (i.e., where the maximum NO release has been observed), $a$ is the soil moisture curve's shape factor (solely derived from NO release and gravimetric soil moisture data which have been observed during the drying-out measurements, see Behrendt et al. 2014), $T_{soil}$ is the soil temperature (in °C), $T_{soil,0}$ is the reference temperature (here: 20°C), and $Q_{10,NO}$ is the (logarithmic) slope of $h(T_{soil})$, defined by

$$Q_{10,NO} = \frac{\ln F_{NO}(\theta_{g,0}, T_{soil,1}) - \ln F_{NO}(\theta_{g,0}, T_{soil,0})}{T_{soil,1} - T_{soil,0}} \quad (7)$$

where $T_{soil,1}$ is a soil temperature which is 10 K different from $T_{soil,0}$ (here: 30°C). The actual NO fluxes $F_{NO}$ (ng m$^{-2}$ s$^{-1}$; in terms of mass of nitric oxide) are defined by

$$F_{NO}(\theta_{g,0}, T_{soil,0}) = \frac{Q}{A_{soil}}\left[m_{NO,cham}(\theta_{g,0}, T_{soil,0}) - m_{NO,ref}\right] f_{C,NO} \quad (8)$$

$$F_{NO}(\theta_{g,0}, T_{soil,1}) = \frac{Q}{A_{soil}}\left[m_{NO,cham}(\theta_{g,0}, T_{soil,1}) - m_{NO,ref}\right] f_{C,NO} \quad (9)$$

where $Q$ is the purging rate of the dynamic chambers (m$^3$ s$^{-1}$), $A_{soil}$ is the cross-section of the dynamic chamber (m$^2$), and $m_{NO,cham}$ and $m_{NO,ref}$ are the NO mixing ratios (ppb) observed under conditions ($\theta_{g,0}$,$T_{soil,0}$) and ($\theta_{g,0}$,$T_{soil,1}$) at the outlets of each soil chamber and the reference chamber, respectively. The conversion of NO mixing ratios to corresponding NO concentrations (ng m$^{-3}$, in terms of mass of nitric oxide) is considered by $f_{C,NO}$ (= 572.5 ng m$^{-3}$ ppb$^{-1}$ under STP conditions). Finally, the net potential NO flux, $F_{NO}(\theta_g, T_{soil})$ is given by

$$F_{NO}(\theta_g, T_{soil}) = F_{NO}(\theta_{g,o}, T_{soil,0})\, g(\theta_g)\, h(T_{soil}) \quad (10)$$

This net potential NO flux is specific for each soil sample, hence for sites (1), (2), (4), and (5) of Milan oasis; the actual NO flux of the sites is calculated applying corresponding field data of gravimetric soil moisture and soil temperature. This procedure has been successfully applied for a variety of terrestrial ecosystems (e.g., Otter et al., 1999; van Dijk et al., 2002; Ganzeveld et al., 2008). For soils of the Zimbabwean Kalahari (Ludwig et al., 2001; Meixner and Yang, 2006), for a German grassland soil (Mayer et al., 2011), but also for Brazilian rainforest soils (van Dijk et al, 2002), soil biogenic NO fluxes derived from the described laboratory incubation method have been successfully verified by field measurements using both, field dynamic chamber and micrometeorological (aerodynamic gradient) techniques.

### 2.2.5 Classification and actual distribution of Milan fields

Image classification is likely to assemble groups of identical pixels found in remotely sensed data into classes that match the informational categories of user interest by comparing pixels to one another and to those of known identity. For the purposes of our study, land-cover classification was carried out based on two Quickbird images (0.6 m ground resolution, DigitalGlobe, http://www.digitalglobe.com) acquired on 09 April and 31 August 2007 respectively, with the aid of a recent ETM+ Landsat image (141/033, http://earthexplorer.usgs.gov/) acquired on 25 April 2011 (15 and 30 m spatial resolution). A major advantage of using Quickbird images of high spatial resolution images is that such data greatly reduce the mixed-pixel problem (a “mixed pixel” consists of several land-cover classes) and provide a greater potential to extract much more detailed information on land-cover structures (e.g. field borders, buildings, roads) than medium or coarse spatial resolution data using whether on screen digitizing or image classification.

However, we take the advantage of resolution merge processing to increase the spatial resolution of the Landsat image from 30 to 15 meters for the bands 1-5 and 7 for better land-cover mapping and for updating the land-cover map from 2007 to 2011. Then, we defined different areas of interests (AOIs) to represent the major land-covers with the aid of in-situ GPS data collection (45 points). Next, we increased number of AOIs based on image spectral analysis method. After that supervised classification was performed using the maximum likelihood parametric rule and probabilities. This classifier uses the training data by means of estimating means and variances of the classes, which are used to estimate Bayesian probability and also consider the variability of brightness values in each class. For that, it is the most powerful classification method when accurate training data is provided and one of the most widely used algorithms (Perumal and Bhaskaran, 2010). As a result, five major

ecosystems were determined: cotton, jujube, cotton/jujube mixture fields, desert, and plant cover. The cotton and the jujube fields are the most dominant types. Finally, the classified land-cover image was converted into vector format using polygon vector data type to be implemented in LASAT analysis as sources of NO flux and for the purpose of estimating NO concentrations. The map includes 2500 polygons of different sizes as sub-units of Milan major land-cover.

### 2.2.6 Two dimensional distribution of soil NO emissions of Milan oasis

The soil NO emission sources of Milan oasis were defined by individual source units, which have been identified as those sub-units (polygons) of the land-cover vector map consisting of natural forest or desert, or covered by cotton, jujube, cotton/jujube mixture. Two identifiers have been attributed to each source unit, (a) a metric coordinate whose numerical format refers to the corner of the corresponding polygon, and (b) a unique ID number followed by a description of its land cover type. The soil NO source strength (i.e., actual NO flux, see Sect. 2.2.4) of each source unit has been calculated from the corresponding net potential NO flux, the land-cover type specific gravimetric soil moisture content ("wilting point"), and the actual soil temperature, which has been *in-situ* measured for each of the land-cover types of Milan oasis (see Sect. 2.2.2). Those polygons which are not matching the mentioned land-cover types and other tiny polygons generated by digital image processing techniques were dismissed to avoid intricate geometric errors affecting NO emission data. In other words, these "other classes" were dissolved before performing LASAT analysis to avoid extreme values.

### 2.2.7 Three dimensional distribution of NO concentrations by Lagrangian dispersion modelling (LASAT)

Having the actual NO source units of the Milan oasis available, the 3-D distribution of NO concentrations in the atmospheric boundary layer (0 – 1500 m a.gr.) over Milan oasis have been calculated by the Lagrangian dispersion model LASAT (German VDI Guidelines VDI3945, part 3; c.f. Janicke Consulting, 2011). LASAT is a state-of-the-art model, since (a) LASAT is one of those transport-dispersion models of air-pollution which is officially licensed for legal use of environmental issues (in Germany), and (b) among comparable micro-scale (e.g. street canyons) transport-dispersion models LASAT considers at least chemical transformations of 1$^{st}$ order and keeps nonetheless truly operational. Being a transport-dispersion-model, LASAT basically considers advection ("pixel cross-talk")

applying the 3D-continuity equation for any chosen tracer (see German VDI Guidelines VDI3945, part 3, cf. Janicke Consulting, 2011). For that, pre-processing of meteorological parameters (i.e. 3-D wind distributions, based on meteorological in-situ measurements, see Sect. 2.2.2) and calculation of dispersion parameters ($\sigma_y$, $\sigma_z$) have to be performed. Unfortunately, it was difficult to obtain fine resolution using LASAT individually. Therefore, LASAT model was integrated with Geographic Information System (ArcGIS) by using an advanced module namely LASarc (IVU Umwelt GmbH, 2012). LASarc allowed us to calculate NO concentrations using relatively fine resolution of 30m×30m and taking the advantages of using integrated map colour scheme in ArcGIS. This module has been used to realize Milan oasis' complex NO source configuration and to setup calculations of LASAT.

The model was designed to calculate NO-concentrations at 16 different vertical layers (0–3, 3–5, 5–10, 10–20, 20–30, 30–50, 50–70, 70–100, 100–150, 150–200, 200–300, 300–400, 400–500, 500–700, 700–1000, and 1000–1500 m a.gr.). The horizontal resolution is 30 m, in x-direction (W-E) as well in y-direction (S-N), which results in 656 (x) and 381 (y) grids for the Milan oasis domain. LASAT's meteorological input data contain a variety of parameters, namely start and end time ($T_1$, $T_2$), wind speed ($U_a$) and wind direction ($R_a$) at anemometer height ($H_a$), average surface roughness ($Z_0$), and atmospheric stability (in terms of stability classes). These parameters have been provided in a time-dependent tabular form, up-dated every 30 minutes (except $Z_0$). Average (30 min) wind speed and wind direction data have been calculated from *in-situ* measurements (1 min resolution, see Sect. 2.2.2).

LASAT's pre-processing module determines the vertical profile of wind speed according to the well-known logarithmic relation,

$$U(z) = \frac{u_*}{k} \ln\left(\frac{z}{Z_0}\right) \qquad (11)$$

where $U(z)$ is the horizontal wind speed (m $s^{-1}$) at height $z$ (m), $u_*$ is the friction velocity (m $s^{-1}$), $k$ is the dimensionless von Karman constant (= 0.4, Simiu and Scanlan, 1996), and $Z_0$ is the surface roughness length (m). LASAT's pre-processing module accepts only one individual value for $Z_0$; nevertheless, the required mean value has been calculated from all $Z_0$'s of Milan oasis domain, which have been assigned to each of the sub-units (polygons) of the vector land-cover map (see Sect. 2.2.5). For individual $Z_0$'s, we calculated land-cover specific NDVI data (normalized differential vegetation index) from Landsat ETM+ image (141/033)

$$NDVI = \frac{r_{NIR} - r_{RED}}{r_{NIR} + r_{RED}} \quad (12)$$

where *NIR* is the reflectance in the near-infrared bandwidth (0.77-0.90 µm) and *RED* is the reflectance in the red bandwidth (0.63-0.69 µm). In Landsat ETM+ images, these correspond to bands 4 and 3, respectively. Finally, $r_{NIR}$ and $r_{RED}$ are the corresponding ratios of reflected and incident energy as a function of wavelength (see Chander and Markham, 2003). Then, surface roughness grid data was estimated as:

$$Z_0(x,y) = \exp\left(a_{xy}\, NDVI(x,y) + b_{xy}\right) \quad (13)$$

where $a_{xy}$ and $b_{xy}$ are constants, which are, according to Morse et al. (2000), derived from *NDVI*(*x,y*) and GPS(x,y) data for known sample pixels representing the earlier classified land-cover types, namely natural forest, desert, cotton, jujube, and cotton/jujube mixture. Corresponding land-cover type $Z_0$'s are 0.45, 0.01, 0.18, 0.26, and 0.22 m, respectively; the required average value over the entire LASAT model domain results in $Z_0 = 0.22 \pm 0.158$ m.
Besides mechanical turbulence ($Z_0$), atmospheric stability affects most the dispersion of trace substances. For Milan oasis' atmospheric boundary layer, atmospheric stability has been calculated according to the "solar radiation/delta T (SRDT)" method in 30 min intervals. This method (c.f. Turner, 1994) is widely accepted because of its simplicity and its representativeness for atmospheric stability over open country and rural areas, like the Milan oasis domain. Daytime stability classes are calculated from *in-situ* measurements of solar radiation and horizontal wind speed (see Sect. 2.2.2).
Finally, 30 min means of all parameters and input variables of LASAT have been calculated. Using these, about $4\times10^6$ gridded data points of 3-D NO concentration have been calculated for each time period considered in Section 3.2.

### 2.2.8 Simulation of $SCD_{NO2}$ and $VCD_{NO2}$ by spatial integration of LASAT results

There is only one tool to provide a robust relationship between biogenic soil NO emissions on one hand and MAX-DOAS observed SCD's and VCD's on the other hand: the exact simulation of the MAX-DOAS measurement through spatial integration of three dimensional NO concentrations calculated by LASAT (followed by $NO \rightarrow NO_2$ conversion). At a given location of the MAX-DOAS measurement, integration must be performed from the height where the MAX-DOAS instrument has been set-up ($h_{MAXDOAS}$) to the end of the atmospheric boundary layer ($h_{ABL}$ = 1500 m a.gr.) along two virtual light paths, (a) the vertical up path

(VCD), and (b) the slant path (SCD) according to the selected elevation angle of each MAX-DOAS measurement.

Calculation of simulated VCD's for NO ($VCD_{NO,sim}$) at the location of a MAX-DOAS instrument is achieved as follows: (a) determination of the NO mass density (ng $m^{-2}$) of the vertical column between $h_{MAXDOAS}$ and $h_{ABL}$; this is obtained by adding NO concentrations (ng $m^{-3}$ in terms of mass of nitric oxide) of all LASAT cells in vertical direction over that 30 m × 30 m grid, which contains the location of the MAX-DOAS instrument, multiplied by the height difference $\Delta h = h_{ABL} - h_{MAXDOAS}$ (in m), (b) multiplying that NO mass density by the ratio of Avogadro's number ($6.02217\times10^{26}$ molecules $kmol^{-1}$) and the molecular weight of NO ($30.0061\times10^{12}$ ng $kmol^{-1}$) delivers the desired value of $VCD_{NO,sim}$ in units of molecules $m^{-2}$ ($\times10^{-4}$: molecules $cm^{-2}$) at the location of the MAX-DOAS instrument. Calculation of simulated SCD's for NO ($SCD_{NO,sim}$) requires the determination of the 3-D light path through the trace gas layered. Positioning of MAX-DOAS's telescope was always to the north, the selected MAX-DOAS elevation angle α and $h_{ABl}$ deliver the length of the slant light path (= $h_{ABL}/\sin\alpha$). The desired $SCD_{NO,sim}$ (in molecules $m^{-2}$) results from the NO mass density of the slant column multiplied by the length of the slant light path, where the NO mass density is equivalent to the sum of all NO concentrations of those LASAT cells which are intersected by the slant light path from the position of the MAX-DOAS instrument to $h_{ABL}$.

For conversion of $VCD_{NO,sim}$ to $VCD_{NO2,sim}$ and $SCD_{NO,sim}$ to $SCD_{NO2,sim}$ it is assumed, that the photostationary state (PSS) of the triad NO, $NO_2$, and $O_3$ is established in Milan oasis' atmospheric boundary layer. According to Leighton (1961) this chemical equilibrium state is due to fast photochemical reactions, namely $NO+O_3 \rightarrow NO_2+O_2$ and $NO_2+h\upsilon \rightarrow NO+O$, from which the so-called photostationary state $NO_2$ concentration ($NO_{2,PSS}$) can be derived as

$$\left[NO_{2,PSS}\right] = \frac{\left[O_3\right]\left[NO\right]k_1}{j\left(NO_2\right)} \quad (14)$$

where $[O_3]$ is the ozone number density (molecules $cm^{-3}$; calculated from *in-situ* measured $O_3$ concentrations, see Sect. 2.2.2), [NO] is the NO number density, $k_1$ is the reaction coefficient of the $NO+O_3 \rightarrow NO_2+O_2$ reaction ($cm^3$ $molecules^{-1}$ $s^{-1}$; Atkinson et al., 2004), and $j(NO_2)$ is the *in-situ* measured $NO_2$ photolysis rate (in $s^{-1}$; see Sect. 2.2.2). Finally, $VCD_{NO2,sim}$ and $SCD_{NO2,sim}$ are calculated from $VCD_{NO,sim}$ and $SCD_{NO,sim}$ by

$$VCD_{NO2,sim} = CF_0 \times VCD_{NO,sim} \text{ and } SCD_{NO2,sim} = CF_0 \times SCD_{NO,sim} \quad (15)$$

where the $NO \rightarrow NO_2$ conversion factor is defined by $CF_0 = [O_3]\, k_1 / j(NO_2)$.

Since the $NO\text{-}NO_2\text{-}O_3$ photochemical equilibrium could not be handled by LASAT's "chemical" algorithm, we decided to use measured data ($O_3$ mixing ratio, $NO_2$ photolysis rate, s. sect. 2.2.2) to convert the calculated 3D-NO mixing ratio to the photo-stationary 3D-$NO_2$ mixing ratio. For that, a constant vertical $O_3$ mixing ratio (up to 1500 m a.gr.) is assumed over Milan oasis. This is justified by the fact, that particularly in arid and hyper-arid landscapes at mid-day conditions (maximum of insulation) the entire atmospheric boundary layer is intensively mixed, which is due to extensive convective heating of the surface by the sun which produces powerful buoyant thermals that establish the so-called mixing layer. Consequently an uniform vertical mixing ratio is expected for trace gases with chemical lifetimes greater than the exchange time of the atmospheric boundary layer. (c.f. Husar et al. 1978, Stull 1988). This assumption is valid for ozone. Vertically constant $O_3$ mixing ratio has been reported for the atmospheric boundary layer over semi-arid southern Africa (Meixner et al., 1993). Concerning the vertical distribution of $j(NO_2)$ it is obvious, that the downward component of the actinic flux increases with increasing elevation due to the decreasing optical thickness of the scattering air masses. However, the altitude effect on the actinic flux in the first kilometer of the troposphere is typically very small. Trebs et al. (2009) used the Tropospheric Ultraviolet Visible model to calculate the typical vertical change of the actinic flux and found a vertical gradient of 1.1%/km. Consequently, our calculations of the NO to $NO_2$ conversion in the boundary-layer over Milan oasis (1500 m a.gr.) have not considered any potential vertical change of the $j(NO_2)$ values measured at ground level. Nevertheless, for the case of our measurements the locally enhanced NO values caused by the soil emissions have a small but systematic effect on the ozone concentration, and thus also on the Leighton ratio: Close to the surface (below about 50m) the NO concentrations can be quite large, with maximum values up to about 10 ppb. Consequently, the ozone concentration will be reduced due to the reaction with NO by up to about 10 ppb. This means that the Leighton ratio will be reduced by up to about 25%. Although the reduction of the ozone mixing ratio wil be partly compensated by mixing with air from higher altitudes, the simulated $NO_2$ mixing ratios might overestimate the true $NO_2$ mixing ratios by up to about 25%. Probably the true overestimation for our measurements is much smaller because the typical NO mixing ratio within the lowest 100m is much lower than 10 ppb.

## 3 Results and Discussion

### 3.1 Land-cover type specific net potential NO fluxes

Net potential NO fluxes (as functions of soil temperature and moisture) have been determined by incubation of samples which have been taken from the top-soil of Milan oasis' major land-cover types, i.e. natural forest, desert, cotton, jujube, and cotton/jujube mixture (see Sect. 2.2.4). Figure 2 shows the laboratory derived net potential NO flux, $F_{NO}$ from soils of the most contrasting land-cover types of Milan oasis (irrigated & fertilized fields of cotton, jujube, cotton/jujube mixture, and desert).

Net potential NO fluxes of the natural forest land-cover type are not shown, because laboratory incubation measurements have shown that there is no significant NO release from these soils, most likely due to its high electrical conductivity (salt content). Optimum gravimetric soil water contents (i.e., where the maximum of $F_{NO}$ is observed) for desert, managed cotton, and managed jujube soils have one in common, very low values of $\theta_{g,opt}$ (0.009–0.017) for soil temperatures of 50°C. During the vegetation period (April – September), soil temperatures of > 40°C are easily reached for the soils of Milan oasis, particularly for the desert soils. While the nature of all Milan oasis' soils is arid/hyper-arid, maximum net potential NO fluxes are 7600, 63, 270, and 98 ng $m^{-2}$ $s^{-1}$ (in terms of mass of nitric oxide) for cotton, jujube, jujube/cotton mixture, and desert soils, respectively.

### 3.2 Land-cover types of Milan oasis and actual NO fluxes

As mentioned in Section 2.2.5, land-cover classification and actual distribution of Milan oasis' fields have been identified from satellite images (Quickbird, Landsat ETM+). The 2011 distribution of fields and the corresponding land-cover is shown in Figure 3.

The dominant crop was cotton, representing 18% (64 $km^2$) of the total field area of Milan oasis (jujube 7%, 28 $km^2$), cotton/jujube mixture 0.89 % (3 $km^2$), natural forest 18% (64 $km^2$), residential area 1.62% (5.5 $km^2$) and desert 52% (174 $km^2$). Land-cover specific, actual NO fluxes (30 min means) from cotton, jujube, cotton/jujube, and desert soils were calculated from corresponding laboratory derived net potential NO fluxes, land-type specific soil moisture and soil temperature data (see Sect. 2.2.6). These NO fluxes (ng $m^{-2}$ $s^{-1}$, in terms of mass of nitric oxide) were then assigned to each individual source unit (i.e. to each of the 2500 polygons of Milan oasis' domain).

For the period 03 to 24 June, 2011, land-cover specific, actual NO fluxes were calculated according to eq.(10) for cotton, jujube, cotton/jujube, and desert soils from corresponding laboratory derived net potential NO fluxes. As input we used land-type specific, measured

soil temperature data as well as land-type specific soil moisture data (so-called "wilting points", s. Sect. 2.2.3). The calculated NO fluxes are shown in Fig. 4 as median diel variation (for the entire period of 03 to 24 June, 2011). Since NO fluxes from Milan cotton fields dominate the total soil biogenic NO emission of the oasis, corresponding medians and quartiles are shown in Fig. 4, while – for the sake of clarity – for jujube, cotton/jujube, and desert only medians are given. Since land-type specific "wilting points" are constant, diel variations of actual NO fluxes mirror directly those of corresponding soil temperatures, showing the daily minimum around 06:00 local time for all four major land-cover types. The maximum of the actual NO-flux, however, is around 13:00 (local time) for jujube, cotton/jujube, and desert soils, and 15:00 local time for cotton. This is due to the growth of the cotton plants: while at the beginning of the experimental period the bare soil surface was nearly 100% exposed to insolation, the growing cotton canopy has shaded great parts of the soil surfacetowards the end of the experimental period . This is also reflected by the skewed distribution of actual NO-fluxes from cotton covered soil, indicated by the daytime non-symmetric inter-quartile range (= upper quartile – lower quartile). As shown in sect. 3.5, actual NO-flux data of 09 June, 2011 (08:30-14:30 local time) were used for the comparison of LASAT and MAX-DOAS results. During this particular day (within the first week of the experimental period), the derived flux for "land-cover cotton" ranged from 15–64 ng $m^{-2}s^{-1}$ (in terms of mass of NO), those for jujube, cotton/jujube, and desert land-covers ranged from 11–13, 6–16, and 6–17 ng $m^{-2}s^{-1}$, respectively. These actual NO fluxes were then assigned to each individual source unit (i.e. to each of the 2500 polygons of Milan oasis' domain). The soil biogenic NO emission from all cotton fields between 08:30 and 14:30 was estimated to 28.7 kg (in terms of mass of NO), equivalent to 76% of the total soil biogenic NO emission of the entire Milan oasis within 6 hours.

### 3.3 Vertical $NO_2$ column densities by MAX-DOAS

We performed 32 individual MAX-DOAS measurements within 21 days of the 2011 field campaign to examine the spatial variation between the observed sites. In Fig. 5, all observed vertical $NO_2$ column densities (in molecules $cm^{-2}$) observed at sites (1) - (4) of Milan oasis are shown in polar coordinates with reference to corresponding wind directions measured *in-situ* at the individual sites.

Wind speeds (30 min means) ranged between 1.5 and 7.7 m $s^{-1}$ and wind direction was mostly (78%) from the northern quadrants (59%, 9%, 13%, and 19% from NE, SE, SW, and NE quadrants, respectively). As expected, highest VCDs ($10^{15}$ – $10^{16}$ molecules $cm^{-2}$) were

observed at site (4) (Milan oasis center), regardless of wind direction. When the wind direction is from the NE quadrant, site (3) (jujube fields) is down-wind of Milan oasis (see Fig.1); then its VCDs are as high as those obtained in the oasis' center ($5 - 7\times10^{15}$ molecules $cm^{-2}$). The few VCD data points of $1\times10^{15}$ molecules $cm^{-2}$ at the jujube site, attributed to winds from SE and SW quadrants, are mainly due to NO emissions from traffic on the National Road 315 which passes the southern margins of Milan oasis. Lowest VCDs ($3\times10^{13} - 3\times10^{14}$ molecules $cm^{-2}$) have been observed at site (1) (natural forest) and site (2) (desert). Alone from these spatially resolved VCD observations in the Milan oasis' domain, the increase of VCD due to the oasis itself can be estimated in the order of at least one order of magnitude.

Fortunately, we have been able to perform simultaneous measurements with two MAX-DOAS instruments at sites (1) and (3) on 09 and 13 June, 2011. Since winds (approx. 3 m $s^{-1}$) were from the NE quadrant during these two days, site (1) has been up-wind, and site (3) downwind of Milan oasis. Corresponding VCD results are shown in Figure 6. $NO_2$ VCDs at the downwind site exceeded those at the upwind site by factors 5 – 9. This difference between downwind and upwind MAXDOAS signals is considered to be a direct measure for the areal increase of ambient $NO_2$ concentration. In the absence of anthropogenic $NO_x$ sources (see Sect. 2.1), this provides first evidence for the considerable impact of the biogenic NO emissions from the fields of Milan oasis.

### 3.4 3-D distribution of ambient NO-concentration

The LASAT model has to be used to calculate the dispersion of soil emitted NO into the atmospheric boundary layer over Milan oasis. An example for the resulting distribution of NO concentration in the first four vertical layers of LASAT (0-3, 3-5, 5-10, and 10-20 m) is shown in Figure 7 (09 June, 2011; 11:30-13:00 local time). The shown results are the mean of three LASAT model runs, since a new LASAT calculation of 3-D distribution of NO concentration is started for every set of meteorological parameters which are provided every 30 min from means of the *in-situ* measured meteorological quantities (see Sect. 2.2.2). During 11:30-13:00, mean wind direction was 15°, 38°, and 50°, wind speed was rather constant (2.60 – 2.67 m $s^{-1}$), and atmospheric stability class has been generally neutral (3.2).

By comparing the NO ambient concentrations, particularly in the first vertical LASAT layer (0 – 3 m) of oasis area with the surrounding desert, it becomes obvious that the great differences of ambient NO concentrations mirror the corresponding differences of actual soil NO fluxes from each source-unit; within this layer calculated mean NO concentrations are 13, 12,

10, and 1 ng $m^{-3}$ (in terms of mass of nitric oxide; or 10.6, 9.8, 8.2, and 0.8 ppb) for the oasis centre, jujube fields, cotton/jujube mixture, and desert, respectively. The value at the oasis center exceeds those over desert by more than an order of magnitude, similar as the corresponding VCD values (see above). As expected under the prevailing conditions of well developed atmospheric turbulence, NO concentrations rapidly decreases with height (see panels "0–3 m", "3–5 m", "5–10 m" in Fig. 7), and with prevailing northerly winds, the NO concentration centre shifting southwards with increasing altitude.

### 3.5 Simulated SCDs and VCDs *vs.* SCDs and VCDs by MAX-DOAS

For those periods where simultaneous "upwind" and "downwind" MAX-DOAS measurements have been performed (09 and 13 June, 2011), corresponding $SCD_{sim}$ and $VCD_{sim}$ have been simulated by suitable vertical integration (see Sect. 2.2.8) of LASAT-calculated 3-D NO concentrations, followed by $NO \rightarrow NO_2$ conversion (based on photostationary state assumption of Milan oasis' atmospheric boundary layer). Since $SCD_{sim}$ and $VCD_{sim}$ represent only that part of true SCDs and VCDs of $NO_2$, which are due to the contribution of the oasis' soil NO emissions, $SCD_{sim}$ and $VCD_{sim}$ are compared to the difference of those SCDs and VCDs which have been simultaneously measured by two MAX-DOAS instruments at corresponding "downwind" and "upwind" sites (see Fig. 8). For elevation angles of 2° and 4°, $SCD_{sim}$ and $\Delta SCD = SCD_{down} - SCD_{up}$ are shown in Figure 8a. In Figure 8b, $VCD_{sim}$ and $\Delta VCD = VCD_{down} - VCD_{up}$ are shown for 15° elevation.

Here it should be noted that in principle the accuracy of the geometric approximation is higher for the high elevation angles than for the lower elevation angles. However, for the specific cases studied here, this is not the case. First, close to the sources, the height of the layer with elevated $NO_2$ is quite low (in our case the bulk of $NO_2$ is located below 100 m). Second, also the aerosol load is usually very low. Thus the probability of scattering events inside the layer of enhanced $NO_2$ is very low, and consequently the accuracy of the geometric approximation is relatively high. To further quantify the associated uncertainties, we performed radiative transfer simulations and found that the deviations from the geometric approximation are similar for the different elevation angles (about 5% for 2°, 3% for 4° and 3% for 15°). However, because of the shorter light paths through the $NO_2$ layer, the relative error caused by the uncertainty of the spectral analysis is higher than for the low elevation angles. Thus for the case of our measurements, we indeed expect lower uncertainties for the low elevation angles.

Since soil NO emission data used in the LASAT dispersion model were calculated from land-cover type specific potential net NO fluxes, which in turn were derived from laboratory incubation experiments on corresponding soil samples, the results in Figure 8 are also considered as an excellent quality assurance of the chosen up-scaling of laboratory results to the oasis scale. There is remarkable good agreement between measured and simulated data.

However, the actual NO emissions (irrespective of the land-cover type) have their maximum in the early afternoon (s. Fig. 4), while the highest height-integrated $NO_2$ concentrations as simulated by LASAT (on the basis of the actual NO emissions) are in the morning (08:30–10:00), followed by rather constant values for the reminder of the day (s. Fig. 8). The apparent discrepancy between both diurnal variations can be simply explained by the diurnal variation of the wind direction and the specific viewing geometry of the MAX-DOAS instrument. The MAX-DOAS instrument was located at the south-west corner of the oasis, and the observations at zenith and low elevation angles probed air masses located at different locations accross the oasis. The wind direction was from north-east in the morning and turned to north-west in the afternoon. Hence, air masses of lower concentration crossed the viewing directions in the afternoon compared to those in the morning. This explains that in spite of the larger $NO_x$ emissions smaller column densities have been observed in the afternoon. The apparent discrepancy of the diurnal cycles of NO emissions and measured $NO_2$ column densities indicates the importance to exactly consider the 3-dimensional $NO_2$ distribution (due to the soil-emitted NO) for the comparison of the model results with MAX-DOAS observations.

The Figure 8b shows that the LASAT simulations overestimate slightly the true $NO_2$ VCD. The both measured and simulated $NO_2$ VSDs have with an average root mean square (RMS) error between the measured and simulated values of approx. 5-15%. However, the overestimation of LASAT simulation is well suited to the fact that in reality a little less NO can be converted to the $NO_2$ because of lower ozone concentration at the surface.

## 4 Conclusion

This study has been focused on the following activities: (1) representative soil sampling from the uppermost soil layer (< 0.05 m) of all land-cover type units (natural forest, cotton fields, jujube fields, cotton/jujube mixture, desert) of Milan oasis (Xinjiang, NW China), (2) laboratory incubation experiments (dynamic chamber system) to characterize the biogenic NO emission from these soil samples in form of net potential NO fluxes as function of soil moisture and soil temperature, (3) determination of the actual size, areal distribution, and land-cover

type of Milan oasis' field units from satellite remote sensing information, (4) field measurements of slant (SCD) and vertical (VCD) $NO_2$ column densities (by MAX-DOAS) and additional quantities (soil moisture, soil temperature, ozone concentration, $NO_2$ photolysis rate, meteorological parameters) during an extended field campaign of 4 weeks at Milan oasis, (5) using data from (2), (3) and (4): calculation of Milan oasis' 2D distribution of actual, land-cover specific NO fluxes, (6) calculation of 3-D NO concentrations in Milan oasis' atmospheric boundary layer originating from the dispersion of biogenic NO soil emissions determined by (5) with help of the Lagrangian dispersion model LASAT, (7) simulation of SCDs and VCDs by suitable vertical integration of calculated 3-D NO concentrations followed by suitable $NO \rightarrow NO_2$ conversion factors derived from *in-situ* measurements, (8) comparison of measured and simulated SCDs and VCDs.

Results of the laboratory derived NO fluxes have shown that the extensively managed (fertilized and efficiently irrigated) cotton fields of Milan oasis release large amounts of soil biogenic NO; NO fluxes range between 10–30 ng $m^{-2}$ $s^{-1}$ (in terms of mass of N), that is approx. 5–10 times more than from a typical central European wheat field (Yamulki et al. 1995; Stohl et al. 1996).

Applying two MAX-DOAS instruments, simultaneous measurements have been performed at upwind and downwind sites of Milan oasis. Downwind site VCDs exceeded those from the upwind site by factors 5 – 9. Differences of VCD and SSC ("downwind" minus "upwind") are a direct measure for the areal increase of ambient $NO_2$ concentration caused by the oasis itself. The measured differences of VCDs and SCDs were compared with the simulated VCDs and SCDs and excellent agreement was found.

This agreement is considered as the first successful attempt to prove the validity of the chosen approach to up-scale laboratory derived biogenic NO fluxes to ecosystem level field conditions, i.e. from the spatial scale of a soil sample ($cm^2$) to field size (ha), and from field size (ha) to the size of an entire (agro-) ecosystem ($km^2$). Furthermore, in the absence of anthropogenic NO sources of Milan oasis (hydropower energy, battery powered trikes), it is obvious, that the areal increase of ambient $NO_2$ concentration in the atmospheric boundary layer of the isolated (in terms of $NO_2$ advection) Milan oasis is entirely due to biogenic NO emission from the arid/hyper-arid soils of the oasis itself. Extensive agricultural management of Milan oasis' crop fields (fertilization (350-600 kg N $ha^{-1}a^{-1}$) and effective irrigation of cotton and jujube fields) obviously provides considerable contribution of biogenic $NO_x$ ($NO+NO_2$) from arid/hyper-arid soils of the Taklimakan desert to the local tropospheric $NO_x$ budget.

About 80% of the Chinese cotton production originates from the 3000 km long belt of oases surrounding Taklimakan Desert ($1.65\times10^6$ $km^2$) in Xinjiang (NW-China); cotton cultivated land area in Xinjiang occupies the first place of entire China. Since 1955, Xinjiang's output of cotton increased 294 times (Lei et al., 2005). Fast economic growth in the region (+11% GDP $a^{-1}$), inevitably accompanied by large anthropogenic $NO_x$ emissions (traffic, energy production), may be countervailed or even exceeded by the "hotspot" character of Xinjiang's oases, namely by soil biogenic NO emissions from agriculturally dominated oases. Most likely, they will contribute most to the regional tropospheric $NO_x$ budget. This is all the more likely, given the continued intensification of oasis agriculture around the Taklimakan desert which will be accompanied by corresponding land use change (desert→dryland farming with irrigation) in the coming decades.

**Acknowledgements**

This work was funded through the German Research Foundation (DFG) project "DEQNO – Desert Encroachment in Central Asia – Quantification of soil biogenic Nitric Oxide" (DFG-MA 4798/1-1), the Max Planck Society (MPG), and the Max Planck Graduate Centre with Johannes Gutenberg-University Mainz (MPGC). The authors like to thank Guozheng Song, Günter Schebeske, Achim Zipka, Yanhong Li, Fanxia Wang, Aixia Yang, Sijun Luo, and Zhilin Zhu for their field assistance and their substantial support before, during, and after the DEQNO 2011 campaign. We also thank Reza Shaiganfar and Steffen Beirle for their supports during the pre-preparation of MAX-DOAS instrument.

**References:**


Ashuri, F.A.: Der Austausch von Stickstoffmonoxid zwischen Boden und Atmosphäre unter besonderer Berücksichtigung des Bodenwassergehaltes, Einfluss kulturlandschaftlicher Verhältnisse auf den Umsatz eines Spurengases. Ph.D. thesis, Johannes Gutenberg University Mainz, Mainz, Germany, 1–169, 2009.

Atkinson, R., Baulch, D.L., Cox, R.A., Crowley, J.N., Hampson, R.F., Hynes, R.G., Jenkin, M.E., Rossi, M.J., Troe, J.: Evaluated kinetic and photochemical data for atmospheric chemistry: Volume I - Gas phase reactions of Ox, HOx, NOx and SOx species, Atmos. Chem. Phys., 4, 1461–1738, 2004.

Bargsten, A., Falge, E., Pritsch, K., Huwe, B., Meixner, F.X.: Laboratory measurements of nitric oxide release from forest soil with a thick organic layer under different understory types, Biogeosciences, 7, 1425–1441, 2010.

Behrendt, T., Veres, P.R., Ashuri, F., Song, G., Flanz, M., Mamtimin, B., Bruse, M., Williams, J., Meixner, F.X.: Characterisation of NO production and consumption: new insights by an improved laboratory dynamic chamber technique, Biogeosciences Discuss., 11, 1187–1275, 2014.

Beirle, S., Platt, U. Wenig, M. and Wagner, T.: Highly resolved global distribution of tropospheric NO2 using GOME narrow swath mode data, Atmos. Chem. Phys., 4, 1913-1924, 2004.

Bogumil, K., Orphal, J., Homann, T., Voigt, S., Spietz, P., Fleischmann, O.C., Vogel,A., Hartmann, A., Kromminga, H., Bovensmann, H., Frerick,J., Burrows, J.P.: Measurements of molecular absorption spectra with the SCIAMACHY pre-flight model: instrument characterization and reference data for atmospheric remote-sensing in the 230–2380 nm region, Journal of Photochemistry and Photobiology A-chemistry, 157(2), 167-184, 2003.

Brinksma, E. J., Pinardi, G. , Volten, H., Braak, R., Richter, A., Schoenhardt, A., Van Roozendael, M. , Fayt, C., Hermans, C., Dirksen, R. J., Vlemmix, T., Berkhout, A.J.C., Swart, D.P. J., Oetjen, H., Wittrock, F., Wagner, T., Ibrahim, O. W., Leeuw, G. de., Moerman, M., Curier, R. L., Celarier, E. A., Cede, A., Knap, W. H., Veefkind, J. P., Eskes, H. J., Allaart, M., Rothe, R., Piters, A. J. M., Levelt, P. F.: The 2005 and 2006 DANDELIONS NO2 and aerosol intercomparison campaigns, Journal of Geophysical Research, Vol. 113, 1-18, 2008.

Chameides, W. L., Fehsenfeld, F., Rodgers, M. O., Cardelino, C., Martinez, J., Parrish, D., Lonneman, W., Lawson, D. R., Rasmussen, R. A., Zimmerman, P., Greenberg, J., Middleton, P., Wang, T.: Ozone precursor relationships in the ambient atmosphere, Journal of Geophysical Research, 92, 6037-6055, 1992.

Chander, G. and Markham, B.: Revised Landsat-5 TM radiometric calibration procedures and postcalibration dynamic ranges, IEEE Transactions on Geoscience and Remote Sensing, 41 (11), 2674-2677, 2003.

Conrad, R.: Soil Microorganisms as controllers of atmospheric trace gases ($H_2$, CO, $CH_4$, COS, $N_2O$ and NO), Microbiological Reviews., 60 (4), 609–640, 1996.

Crutzen, P. J. (1987): Role of the tropics in atmospheric chemistry, in: The Geophysiology of Amazonia, Dickinson, R.E. (ed.), pp. 107-132, 1987, John Wiley & Sons, New York.

Davidson, E. A., Kingerlee, W.: A global inventory of nitric oxide emissions from soils, Nutrient Cycling in Agroecosystems, 48, 37–50, 1997.

Denman, K.L., Brasseur, G.P., Chidthaisong, A., Ciais, P., Cox, P.M., Dickinson, R.E., Hauglustaine, D., Heinze, C., Holland, E.A., Jacob, D.J., Lohmann, U., Ramachandran, S., Da Silva Dias, P.L., Wofsy, S.C., Zhang, X.: Couplings between changes in the climate system and biogeochemistry, in Climate Change 2007: The physical science basis. contribution of working group 1 to the fourth assessment report of the Intergovernmental

751 Panel on Climate Change, edited by Solomon, S., Qin, D., Manning, M., Chen, Z.,
752 Marquis, M., Averyt, K.B., Tignor, M., Miller, H.L., Cambridge University Press,
753 Cambridge, 499-588, 2007.
754 Feig, G.T.: Soil Biogenic Emissions of Nitric Oxide from Arid and Semi-Arid Ecosystems,
755 PhD thesis, Johannes Gutenberg University Mainz, Mainz, Germany, 1–222, 2009.
756 Feig, G.T., Mamtimin, B., Meixner, F. X.: Soil biogenic emissions of nitric oxide from a
757 semiarid savanna in South Africa, Biogeosciences, 5, 1723–1738, 2008a.
758 Feig, G.T., Mamtimin, B., Meixner, F. X.: Use of laboratory and remote sensing techniques to
759 estimate vegetation patch scale emissions of nitric oxide from an arid Kalahari savanna,
760 Biogeosciences Discuss., 5, 4621–4680, 2008b.
761 Galbally, I.E., Johansson, C.: A model relating laboratory measurements of rates of nitric
762 oxide production and field measurements of nitric oxide emissions from soils, Journal of
763 Geophysical Research, 94, 6473- 6480, 1989.
764 Ganzeveld, L., Eerdekens, G., Feig, G.T., Fischer, H., Harder, H., Königstedt, R., Kubistin,
765 D., Martinez, M., Meixner, F.X., Scheeren, B., Williams, J., Lelieveld, J.: Boundary layer
766 exchanges of volatile organic compounds, nitrogen oxides and ozone during the GABRIEL
767 campaign, Atmospheric Chemistry and Physics, 8, 6223-6243, 2008.
768 Gelfand, I., Feig, G., Meixner, F.X., Yakir, D.: Afforestation of semi-arid shrubland reduces
769 biogenic NO emission from soil, Soil Biology and Biochemistry 41, 1561–1570, 2009.
770 Harrison, P., Pearce F.: Deserts and Drylands, AAAS Atlas of Population and Environment,
771 pp. 131-134, 2000. University of California Press, Berkeley, USA.
772 Hartge, H., Horn, R.: Die physikalische Untersuchung von Böden: Praxis Messmethoden
773 Auswertung. Schweizerbart-sche Verlagsbuchhandlung, Stuttgart, 1-178, 2009.
774 Hermans, C., Vandeale, A.C., Carleer, M., Fally, S., Colin, R., Jenouvrier, A., Coquart, B.,
775 Merienne, M. F.: Absorption Cross-Sections of Atmospheric Constituents, $NO_2$, $O_2$, and
776 $H_2O$, Environ. Sci. Pollut. Res., 6, 151-158, 1999.
777 Hönninger, G. and Platt, U.: The Role of BrO and its Vertical Distribution during Surface
778 Ozone Depletion at Alert, Atmos. Environ., 36, 2481–2489, 2002.
779 Hönninger, G., von Friedeburg, C., and Platt, U.: Multi Axis Differential Optical Absorption
780 Spectroscopy (MAX-DOAS), Atmos. Chem. Phys., 4, 231–254, 2004.
781 Husar, R.B., Patterson, D.E., Husar, J.D., Gillani, N.V., Wilson Jr., W.E. (1978), Sulfur
782 budget of a power plant plume, Atmospheric Environment, 12 (1-3), 549-568.
783 IVU Umwelt GmbH: LASarc – GIS integration of LASAT, Environmental Planning and
784 Information Systems, Freiburg, Germany, 2012.
785 Janicke Consulting: Dispersion model LASAT, Version 3.2, Reference Book. Janicke
786 Consulting, Überlingen, Germany, 239 p, 2011.
787 Kargas, G., Ntoulas, N., Nektarios, P.A.: Soil texture and salinity effects on calibration of
788 TDR300 dielectric moisture sensor. Soil Research, 51 (4), 330-340, 2013.
789 Kirkman, G.A., Yang, W.X., Meixner, F.X.: Biogenic nitric oxide emissions upscaling: An
790 approach for Zimbabwe, Global Biogeochem. Cycles, 15, 1005–1020, 2001.
791 Koeppen, W.: Grundriss der Klimakunde. Gruyter Verlag, Berlin/Leipzig, Germany, 388 p,
792 1931.
793 Kottek, M., Grieser, J., Beck, C., Rudolf, B. and Rubel, F.: World Map of the Köppen-Geiger
794 climate classification Updated, Meteorologische Zeitschrift, 15 (3), 259-263, 2006.
795 Kurucz, R. L., Furenlid, I., Brault, J., Testerman, L.: Solar Flux Atlas from 296 nm to 1300
796 nm, National Solar Observatory Atlas No. 1, 1984. Office of University publisher, Harvard
797 University, Cambridge.

Lei, J., Zhang, X. L.: Structural Adjustment of Oasis Agriculture in Xinjiang, Chinese Journal of Population, Resources and Environment, 3 (3), 29-33, 2005.

Leighton, P. A.: Photochemistry of Air Pollution, Academic Press, New York and London, 300 p, 1961.

Leue, C., Wenig, M., Wagner, T., Platt, U., Jähne, B.: Quantitative analysis of $NO_x$ emissions from GOME satellite image sequences, J. Geophys. Res., 106, 5493-5505, 2001.

Ludwig, J., Meixner, F.X., Vogel, B., Förstner, J.: Processes, influencing factors, and modelling of nitric oxide surface exchange—an overview, Biogeochemistry, 52 (3), 225-257, 2001.

Mayer, J.-C., Bargsten, A., Rummel, U., Meixner, F.X., Foken, T.: Distributed modified bowen ratio method for surface layer fluxes of reactive and non-reactive trace gases, Agricultural and Forest Meteorology, 151, 655-668, 2011.

Meixner, F.X., Ajavon, A.-L., Helas, G., Scharffe, D., Zenker, T., Harris, G.W., Andreae, M.O. (1993), Vertical distribution of ozone over southern Africa: Airborne measurements during SAFARI-92, AGU Fall Meeting, San Francisco, U.S.A.

Meixner, F.X., Yang, W.X.: Biogenic emissions of nitric oxide and nitrous oxide from arid and semiarid land, in: Dryland Ecohydrology, edited by: D'Odorico, P. and Porporat, A., Springer, Dordrecht, the Netherlands, 233–255, 2006.

Morse, A., Tasumi, M., Allen, R. G., and Kramber, W. J. (2000): Application of the SEBAL Methodology for Estimating Consumptive Use of Water and Streamflow Depletion in the Bear River Basin of Idaho through Remote Sensing, Final report submitted to The Raytheon Systems Company, Earth Observation System Data and Information System Project, Boise, USA, 107 pp., 2000.

Otter, L.B., Yang, W.X., Scholes, M.C., Meixner, F. X.: Nitric Oxide emissions from a southern African Savannah, J. Geophys. Res., 104, 18471–18485, 1999.

Perumal, K. and Bhaskaran, R.: Supervised classification performance of multispectral images. Journal of Computing, 2-2, 124-129, 2010.

Platt, U. and Stutz, J.: Differential Optical Absorption Spectroscopy: Principles and Appications, Springer, Berlin, Heidelberg, Germany, 135–377, 2008.

Rothman, L.S., Jacquemart, D., Barbe, A., Chris Benner, D., Birk, M., Brown, L.R., Carleer, M.R., Chackerian Jr, C., Chance, K., Coudert, L.H., Dana, V., Devi, V.M., Flaud, J.-M., Gamache, R.R., Goldman, A., Hartmann, J.-H., Jucks, K.W., Maki, A.G., Mandin, J.-Y., Massie, S.T., Orphal, J., Perrin, A., Rinsland, C.P., Smith, M.A.H., Tennyson, J., Tolchenov, R.N., Toth, R.A., Vander Auwera, J., Varanasi, P., Wagner, G.: The HITRAN 2004 molecular spectroscopic database, Journal of Quantitative Spectroscopy & Radiative Transfer, 96, 139-204, 2005.

Rudolph, J., Conrad, R.: Flux between soil and atmosphere, vertical concentration profiles in soil, and turnover of nitric oxide: 2. Experiments with naturally layered soil cores, Journal of Atmospheric Chemistry, 23, 275-300, 1996.

Rudolph, J., Rothfuss, F., Conrad, R.: Flux between soil and atmosphere, vertical concentration profiles in soil, and turnover of nitric oxide: 1. Measurements on a model soil core, Journal of Atmospheric Chemistry, 23, 253−273, 1996.

Richter, A., Burrows, J.P.: Tropospheric NO2 from GOME Measurements, Adv. Space Res., 29(11), 1673-1683, 2002.

Simiu, E., Scanlan, R.H.: Wind Effects on Structures: Fundamentals and Applications to Design, Third Edition, John Wiley & Sons, New York, USA, 704 p., 1996.

Sinreich, R., Frieß, U., Wagner, T., Platt, U.: Multi axis differential optical absorption spectroscopy (MAX-DOAS) of gas and aerosol distributions, Faraday Discuss., 130, 153–164, doi:10.1039/b419274p, 2005.

Solomon, S., Schmeltekopf, A. L., Sanders, R. W.: On the interpretation of zenith sky absorption measurements, J. Geophys. Res., 92, 8311–8319, 1987.

Stohl, A., Williams, E., Wotawa, G. and Kolb, H.K.: A European Inventory of Soil Nitric Oxide Emissions and the Effect of these Emissions on the Photochemical Formation of Ozone, Atmospheric Enviroment, 30 (22), 3741–3755, 1996.

Stull, R.B. (1988), An Introduction to Boundary-Layer Meteorology, Kluwer Academic Publishers, Dordrecht, The Netherlands. Trebs, I., Bohn, B., Ammann, C., Rummel, U., Blumthaler, M., Königstedt, R., Meixner, F. X., Fan, S., Andreae, M.O. (2009), Relationship between the $NO_2$ photolysis frequency and the solar global irradiance, Atmospheric Measurement Techniques, 2, 725–739

Turner, D.B.: Workbook of atmospheric dispersion estimates. 2nd ed., Lewis publisher, London, 175 p, 1994.

van Dijk, S., Meixner, F.X.: Production and consumption of NO in forest and pasture soils from the amazon basin, Water Air Pollut.-Focus, 1, 119–130, 2001.

van Dijk, S.M., Gut, A., Kirkman, G.A., Meixner, F. X., Andreae, M.O., Gomes, B. M.: Biogenic NO emissions from forest and pasture soils: relating laboratory studies to field measurements, J. Geophys. Res., 107, LBA 25-1–LBA 25-11, doi:10.1029/2001JD000358, 2002.

Vandaele, A.C. Hermans, C. Simon, P.C. Roozendael, M. Carleer, J.M. and Colin, R.: Fourier transform measurement of $NO_2$ absorption cross-section in the visible range at room temperature, J. Atmos. Chem., 25, 289-305, 1996.

Volkamer, R., Spietz, P., Burrows, J., Platt, U.: High-resolution absorption cross-sections of glyoxal in the UV-vis and IR spectral ranges, Journal of Photochemistry and Photobiology A: Chemistry,172 (1), 35-46, 2005.

Wagner, T., Ibrahim, O., Shaiganfar, R., Platt, U.: Mobile MAX-DOAS observation of tropospheric trace gases, Atmos. Meas. Tech., 3, 129-140, 2010.

Wagner, T., Beirle, S., Brauers, T., Deutschmann, T., Frieß, U., Hak, C., Halla, J. D., Heue, K. P., Junkermann, W., Li, X., Platt, U., and Pundt-Gruber, I.: Inversion of tropospheric profiles of aerosol extinction and HCHO and $NO_2$ mixing ratios from MAX-DOAS observations in Milano during the summer of 2003 and comparison with independent data sets, Atmos. Meas. Tech., 4, 2685-2715, doi:10.5194/amt-4-2685-2011, 2011.

Wittrock, F., Oetjen, H., Richter, A., Fietkau, S., Medeke, T., Rozanov, A., Burrows, J. P.: MAX-DOAS measurements of atmospheric trace gases in Ny-Ålesund – Radiative transfer studies and their application, Atmos. Chem. Phys., 4, 955–966, 2004.

Yang, W. X., Meixner, F. X.: Laboratory studies on the release of nitric oxide from subtropical grassland soils: the effect of soil temperature and moisture, in: Gaseous Nitrogen Emissions from Grasslands, Wallingford, England, 67–70, 1997.

Yamulki, S., Goulding, K.W.T., Webster, C.P. and Harrison, R.M.: Studies on NO and $N_2O$ Fluxes from a Wheat Field, Atmospheric Enviroment, 29 (14), 1627–1635, 1995.

Yu, J., Meixner, F. X., Sun, W., Liang, Z., Chen, Y., Mamtimin, B., Wang, G., and Sun, Z.: Biogenic nitric oxide emission from saline sodic soils in a semiarid region, northeastern China: a laboratory study, J. Geophys. Res., 113, 1–11, 2008.

Yu, J., Meixner, F. X., Sun, W., Mamtimin, B., Wang, G., Qi, X., Xia, C., and Xie, W.: Nitric oxide emissions from black soil, northeastern China: a laboratory study revealing significantly lower rates than hiterto reported, Soil Biol. Biochem., 42, 1784–1792, 2010a.

892 Yu, J., Meixner, F.X., Sun, W., Mamtimin, B., Xia, C., Xie, W.: Biogenic nitric oxide
893 emission of mountain soils sampled from different vertical landscape zones in the
894 Changbai Mountains, Northeastern China, Environ. Sci. Technol., 44, 4122–4128, 2010b.
895

**Figures:**

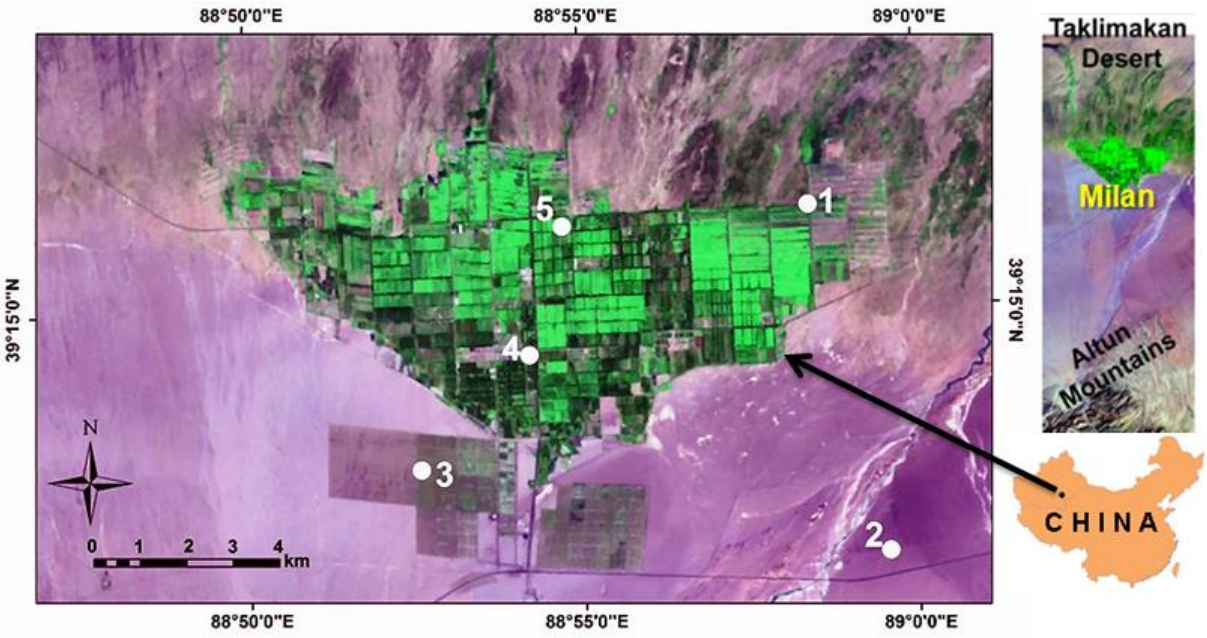


**Fig. 1**: Satellite map (Landsat ETM+; 2011) of Milan oasis, Xinjiang, NW-China (The map has an area of 338 km$^2$). The white circles show the sites of *in-situ* measurements: natural forest (1), desert (2), jujube (3), hotel/oasis station (4) and cotton field (5).

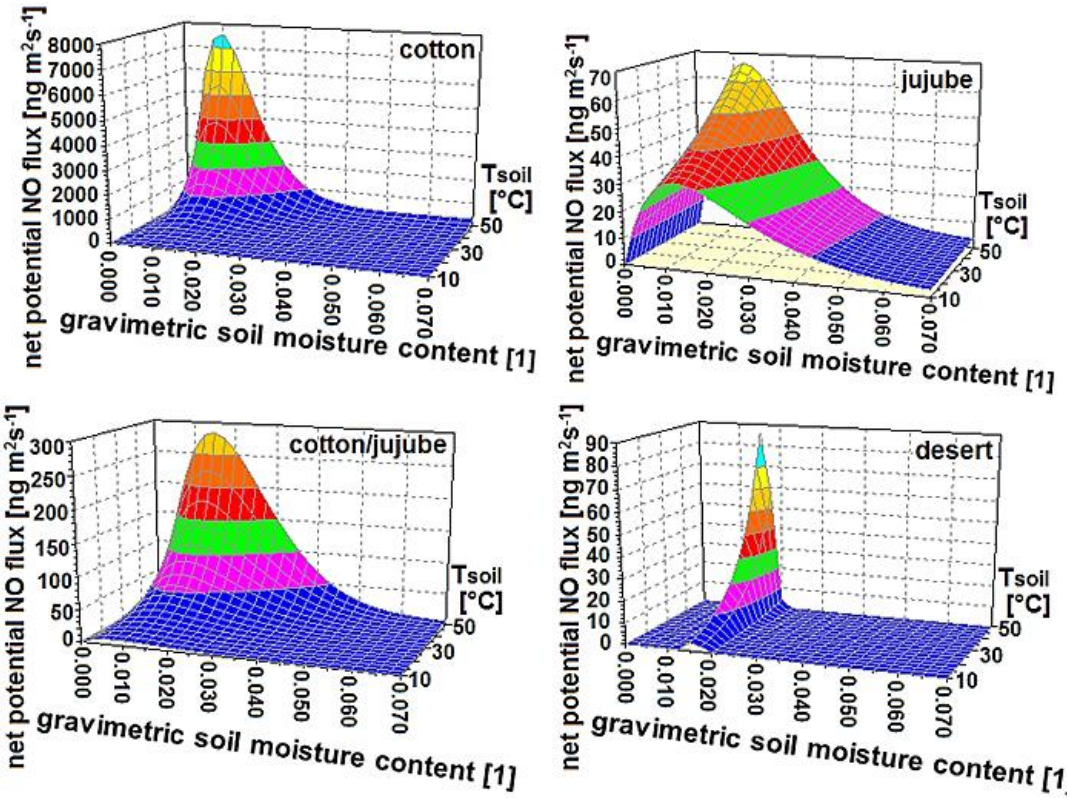


**Fig. 2**: Net potential NO fluxes $F_{NO}$ (ng m$^{-2}$ s$^{-1}$; in terms of mass of nitric oxide) from soils of the four major land-cover types of Milan oasis as functions of soil temperature (°C) and dimensionless gravimetric soil moisture content.

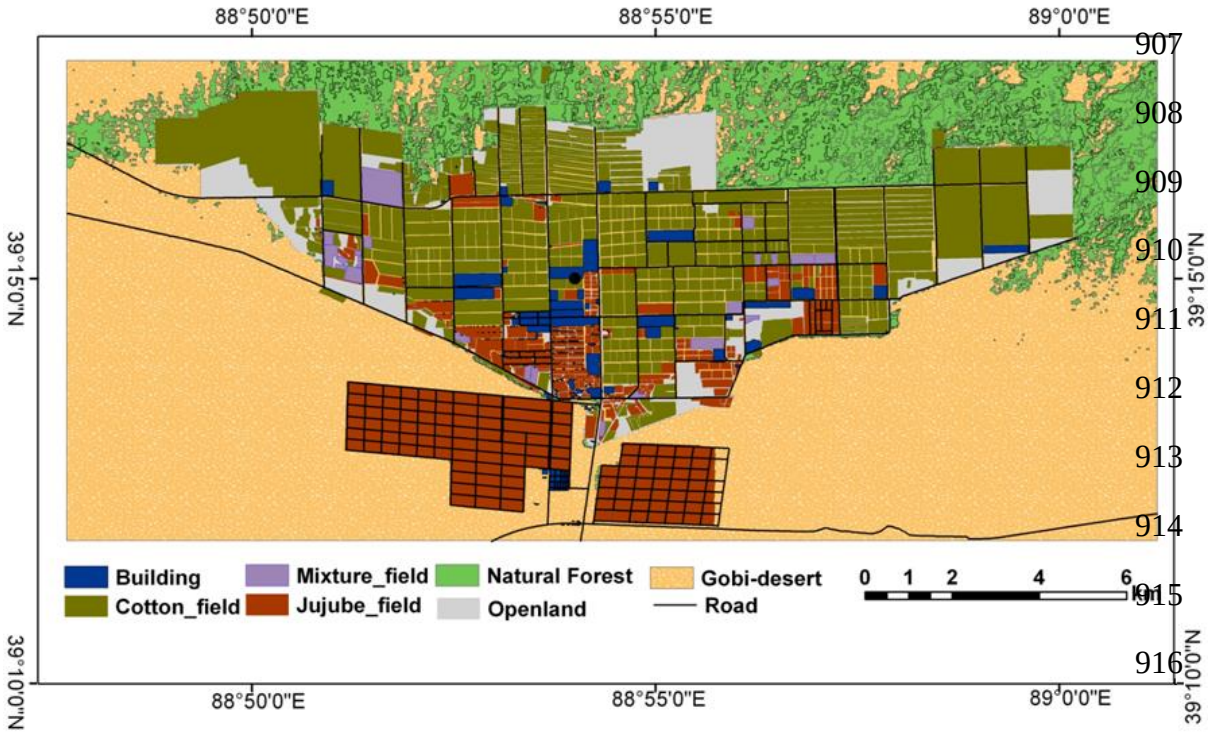


**Fig. 3**: 2011 map of land-cover types of Milan oasis as derived from satellite images (Quickbird, Landsat ETM+, see Sect. 2.2.5).

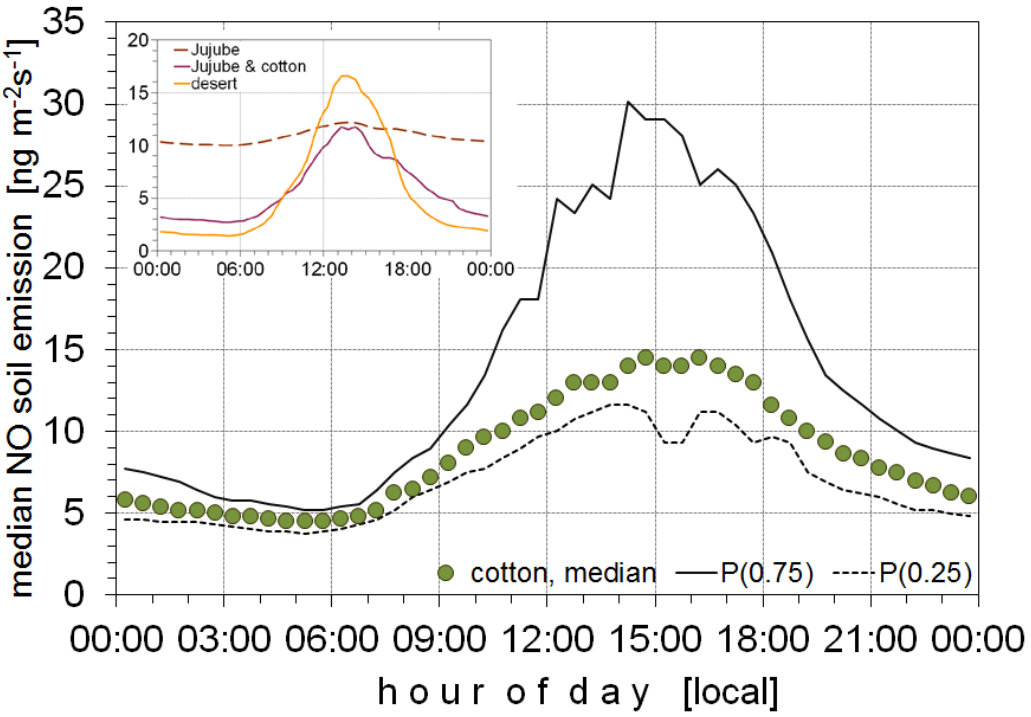


**Fig 4**: median diel variation of the actual NO-flux (ng $m^{-2}s^{-1}$; in terms of mass of nitric oxide) from soils of the four major land-cover types of Milan oasis for the period 03 to 24 June, 2011. Data have been calculated according eq.(10) using (a) soil temperatures (medians) measured for each of the four major land-cover types, and (b) so-called "wilting point"-data for corresponding soil moisture contents at the four sites (s. section 2.2.3). Data for the

cotton-site are given as medians, as well as 25 and 75% quantiles, those for the Jujube, Jujube-cotton and desert sites as medians only (s. figure insert).

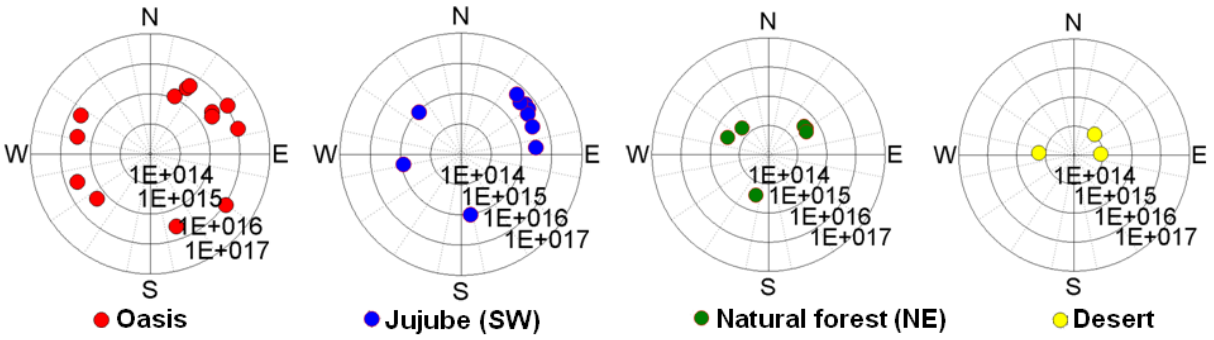


**Fig. 5**: Results of MAX-DOAS measurements performed at sites oasis/hotel (4), Jujube (3), Natural forest (1), and Desert (2) of Milan oasis from 23 May to 26 June, 2011 (see Fig. 1). Vertical $NO_2$ column densities (in molecules $cm^{-2}$; 20-30 min averages) are shown in relation to in-situ measured wind direction at each location of MAX-DOAS measurements. The MAX-DOAS measurements were performed between 6:00 and 19:00 (local time). Note the radial logarithmic scale of VCD data.

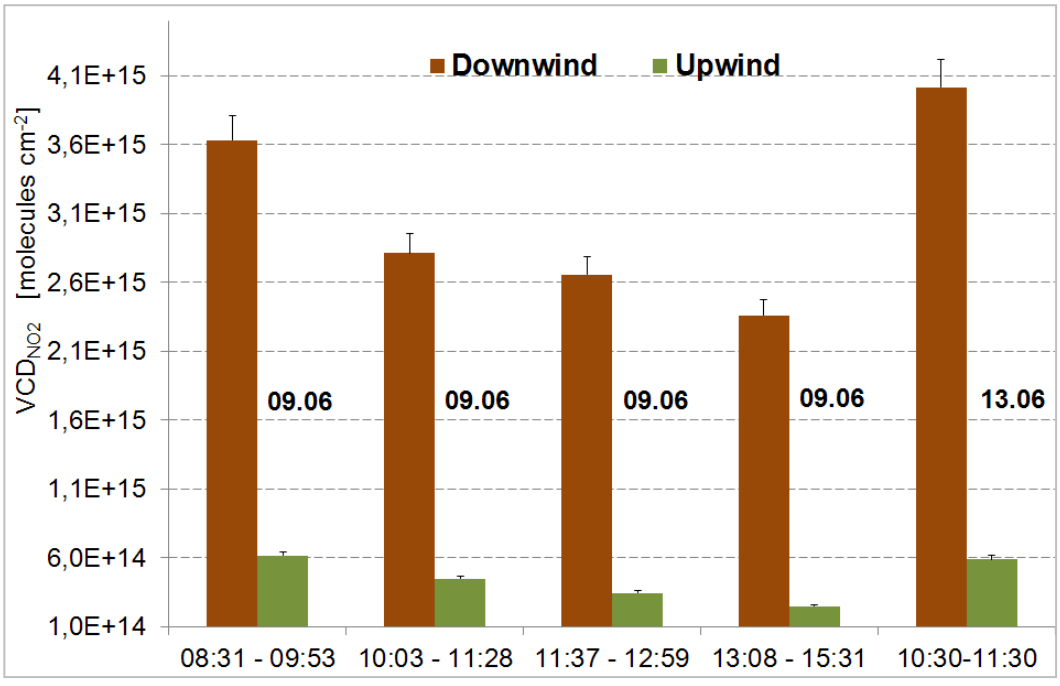


**Fig. 6**: Results of $NO_2$-VCD measured simultaneously with two MAX-DOAS instruments upwind (natural forest, site (1)) and downwind (jujube field, site (3)) of Milan oasis on 09 and 13 June, 2011.

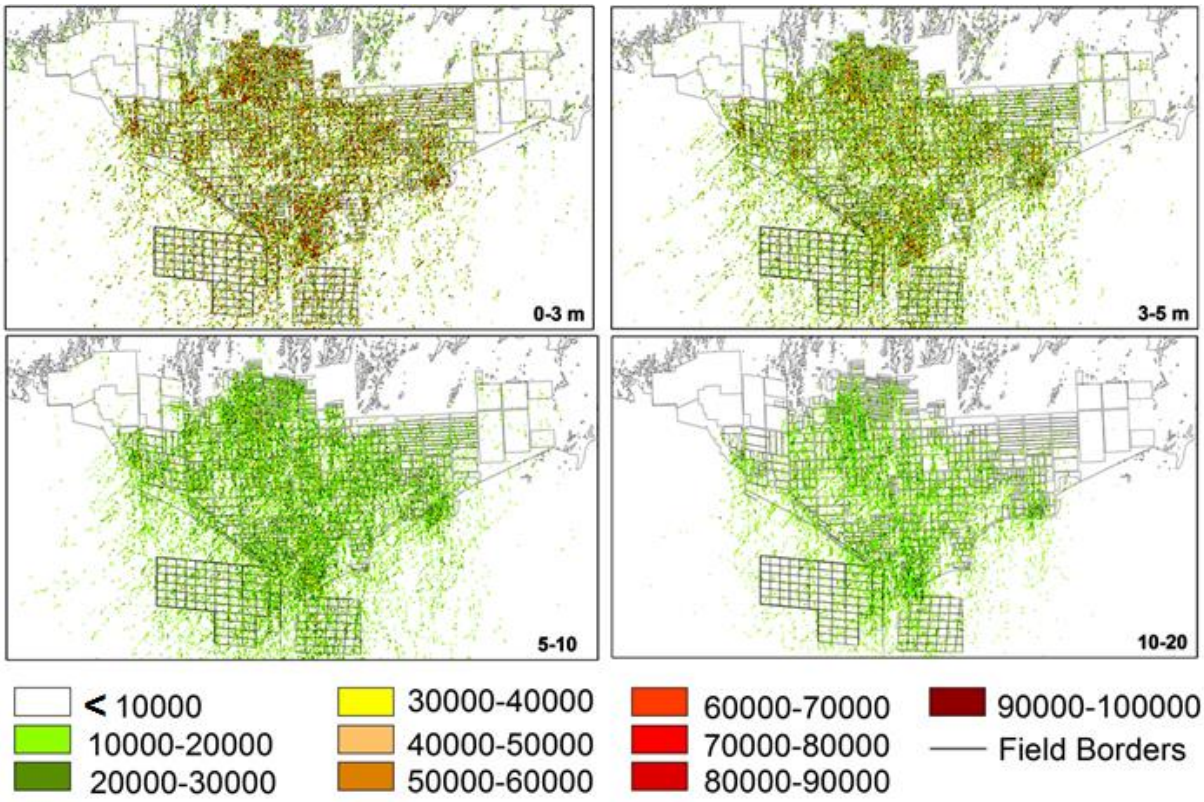


**Fig. 7**: Results of NO concentrations (ng $m^{-3}$; in terms of mass of nitric oxide) calculated by the LASAT dispersion model for the first four vertical levels on 09 June, 2011, 11:30 to13:00 (local time).

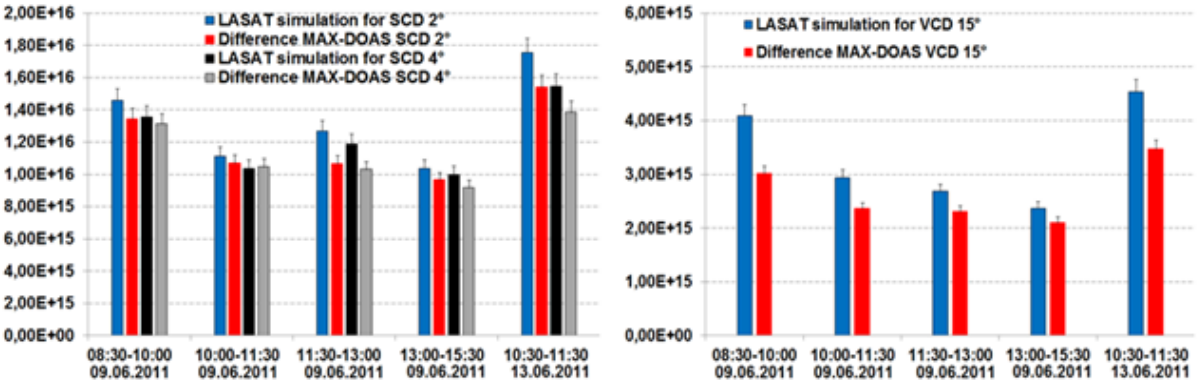


**Fig. 8**: Simulated SCDs vs. SCDs measured by MAX-DOAS (a) and simulated VCDs vs. VCDs measured by MAX-DOAS (b) on 09 and 13 June, 2011 at Milan oasis. SCDs have been measured and simulated for elevation angles of 2° and 4°, VCDs were measured at 15°.